Lithuanian Journal of Physics, Vol. **47**, No. 1, pp. 87–95 (2007) doi:10.3952/lithjphys.47105

XPS AND ELECTRONIC STRUCTURE OF $TlInSe_2$ CRYSTALS

J. Grigas [a], E. Talik [b], M. Adamiec [b], V. Lazauskas [c], and V. Nelkinas [c]

[a] *Faculty of Physics, Vilnius University, Saulėtekio 9, LT-10222 Vilnius, Lithuania*
E-mail: jonas.grigas@ff.vu.lt
[b] *Institute of Physics, Silesian University, Universytetska 4, PL-40007 Katowice, Poland*
[c] *Vilnius University Research Institute of Theoretical Physics and Astronomy, A. Goštauto 12, LT-01108 Vilnius, Lithuania*

Received 19 January 2007

The paper presents the X-ray photoelectron spectra (XPS) of the valence band (VB) and of the principal core levels (CL) from the (010) and (001) plane axes for the quasi-one-dimensional $TlInSe_2$ single crystal. The XPS were measured with monochromatized Al K_α radiation in the energy range of 0–1400 eV at room and 393 K temperature. The VB is located 0.6–10 eV below the Fermi level. Experimental energies of the VB and CL are compared with the results of quantum mechanical *ab initio* calculations of the molecular model of the $TlInSe_2$ crystal. The electronic structure of the VB and CL is described theoretically by quantum mechanical Hartree–Fock calculations. The surface and bulk atoms influence the shape of the VB and CL, which is crystallographic plane dependent. The chemical shifts in the $TlInSe_2$ crystal for the Tl, In, and Se states are obtained.

Keywords: $TlInSe_2$, XPS, electronic structure

PACS: 77.84.-s, 79.60.-i

1. Introduction

Low-dimensional chalcogenides are characterized by a "friable" crystal lattice of a complicated chemical bonding. The structural anisotropy affects lattice and electronic properties. Many of them possess various phase transitions, extreme dielectric and electronic properties [1]. The $TlInSe_2$ is a ternary chain crystal [2]. The chain character of its structure derives from the presence of two inequivalent cation sites. In is in a tetragonal site, while Tl is in an octahedral site. The In and Se atoms form covalent chains along the [001] axis. These chains are held together by weaker ionic bonds through the octahedrically coordinated Tl atoms.

The electronic properties of $TlInSe_2$ are strongly influenced by its nearly molecular character. The crystal can be written as $Tl^{1+}(In^{3+}Se_2^{2-})$. This emphasizes that the crystal contains chains of trivalent In covalently bound to Se, which in turn are ionically bound to monovalent Tl. Such chains form a tetragonal lattice of the space group D_{4h}^{18} (I4/mcm). The crystal exhibits many nonlinear effects, such as S-type characteristics with voltage oscillations, switching, and memory, which attract the interest for technological applications [3, 4].

XPS of binary thallium chalcogenides are discussed in [5]. The electronic structure of $TlInSe_2$ studied by synchrotron radiation photoemission [6] was interpreted in terms of the inequivalent sites for two cations. The CL of Tl $5d$ and In $4d$ are included into VB. However, due to the lack of theoretical calculations of VB structure and CL energies, the width of VB and its electronic structure remain unclear.

Following the previous X-ray photoelectron spectroscopy of the low-dimensional chalcogenides (Bi_2S_3 [7], $TlInS_2$ [8], SbSI [9]) we investigated for the first time the electronic structure of $TlInSe_2$ together with theoretical *ab initio* calculations in greater detail. In literature, there were some indications that at about 370 K a phase transition exists as in other monoclinic ternary thallium chalcogenides [1]. Therefore, XPS were measured at room temperature (RT) and at 393 K.

The organisation of the paper is as follows. A brief description of the experimental details is given in Section 2. In Section 3, a molecular model of the $TlInSe_2$ crystal and *ab initio* calculations of the photoionization energies by the Unrestricted Hartree–Fock (UHF) method are presented and compared with the experimental findings. Section 4 presents experimental results of XPS in $TlInSe_2$ crystal. In Section 5, the experimental and theoretical results are discussed. Finally, conclusions are given in Section 6.

ISSN 1648-8504

2. Experiment

The $TlInSe_2$ crystals were grown from the melt by the Bridgman technique. The XPS of the VB and principal CL were measured with monochromatic Al K_α radiation (1486.6 eV) using PHI 5700/660 Physical Electronics Spectrometer. The photoelectron spectra as functions of kinetic energy were analysed in the range of 0–1400 eV by a hemispherical mirror analyzer. The measurements were performed on the (010) (broken lengthwise) and (001) (broken crosswise) crystal surfaces. The crystal was cleaved *in situ* under ultrahigh vacuum conditions, at a pressure of the low 10^{-10} Torr range, to obtain a clean surface. Like other low-dimensional crystals, cleaved $TlInSe_2$ has limited chemical reactivity. The working pressure was sufficient to keep the sample free of detectable contamination for the duration of the experiment. The only contaminant was found to be carbon. No other spectral features showing non-stoichiometry or impurities have been found. The size of the X-ray spot was about several square microns. The 45 ° angle between the sample and X-ray incident beam was used to analyse the XPS. The sample charging was negligible. For calibration, the carbon C $1s$ (284.5 eV) peak was applied.

3. Molecular model of $TlInSe_2$ crystal and *ab initio* calculation of the energy levels

The electronic structure of the VB and CL was calculated by the method based on Hartree–Fock (HF) matrix equations solution, in the Linear Combinations of Atomic Orbitals (LCAO) approach for the molecular orbitals. According to the Koopmans' theorem, the one-electron energies obtained from the canonical HF equations correspond to the approximate energies of the ionisation potential. Koopmans' theorem applies if the number of electrons in the system is large. Then adding or removing a single electron from the system will not affect the orbitals of the other electrons and they can be assumed fixed.

For the theoretical *ab initio* calculation of energy levels the molecular model of the $TlInSe_2$ crystal is needed. The model must be a cluster composed from an even number of molecules. The interactions between the clusters are not weak, however, as they should be.

Figure 1 shows a fragment of the crystal structure on the xy plane. The unit cell is shadowed. It came out that the stable UHF solution gives the quasi-two-dimensional $z = 1/4c$ plane model. The irreducible cluster of this model is $TlIn_4Se_{16}$. The extension of the cluster in this plane to $Tl_3In_6Se_24$ or $Tl_7In_{10}Se_{40}$ also gives slowly convergent stable solutions of UHF equations. But clusters of other quasi-two dimensional layers with the Miller indices (110) or (100) give unstable solutions of UHF equations.

Table 1. The unit cell atom coordinates.

	X (nm)	Y (nm)	Z (nm)
Tl1	0.0	0.0	0.17118
Tl2	0.0	0.0	0.513555
Tl3	0.403765	0.403765	0.17118
Tl4	0.403765	0.403765	0.513555
In1	0.403765	0.0	0.17118
In2	0.403765	0.0	0.513555
In3	0.0	0.403765	0.17118
In4	0.0	0.403765	0.513555
Se1	−0.138451	0.265314	0.34237
Se2	0.138451	0.265314	0.0
Se3	−0.265314	−0.138451	0.34237
Se4	−0.265314	0.138451	0.0
Se5	0.138451	−0.265314	0,34237
Se6	−0.138451	−0.265314	0.0
Se7	0.265314	0.1384510	0.34237
Se8	0.2653140	−0.138451	0.0

View of the selected cluster $TlIn_4Se_{16}$ of $TlInSe_2$ crystal is framed by an octagon. Table 1 presents the unit cell coordinates. Other coordinates can be obtained by translations. The lattice parameters a and c are 8.0753 and 6.8474 Å, respectively [10].

Such a cluster was used for theoretical calculations. The cluster has an odd number of electrons. The HF method used in [7–9] is inapplicable. For the chosen model we used the Unrestricted Hartree–Fock (UHF) method.

The molecular orbital φ_i (MO) can be expanded as a linear combination of atomic orbitals χ_μ (AO), however, the MO with spin α is not equal to MO with spin β:

$$\varphi_i^\alpha(\mathbf{r}) = \sum_{\mu=1}^{M} C_{i\mu}^\alpha \chi_\mu(\mathbf{r}) \,, \tag{1}$$

$$\varphi_i^\beta(\mathbf{r}) = \sum_{\mu=1}^{M} C_{i\mu}^\beta \chi_\mu(\mathbf{r}) \,, \tag{2}$$

where μ is the number of the AO, or the set of quantum numbers nlm. The coefficients $C_{i\mu}^\alpha$ and $C_{i\mu}^\beta$ in Eqs. (1), (2) and state energies ε_α and ε_β are obtained by solving UHF matrix equations

$$\mathbf{F}^\alpha \, \mathbf{C}^\alpha = \mathbf{S} \, \mathbf{C}^\alpha \, \boldsymbol{\varepsilon}_\alpha \,, \tag{3}$$

$$\mathbf{F}^\beta \, \mathbf{C}^\beta = \mathbf{S} \, \mathbf{C}^\beta \, \boldsymbol{\varepsilon}_\beta \,, \tag{4}$$

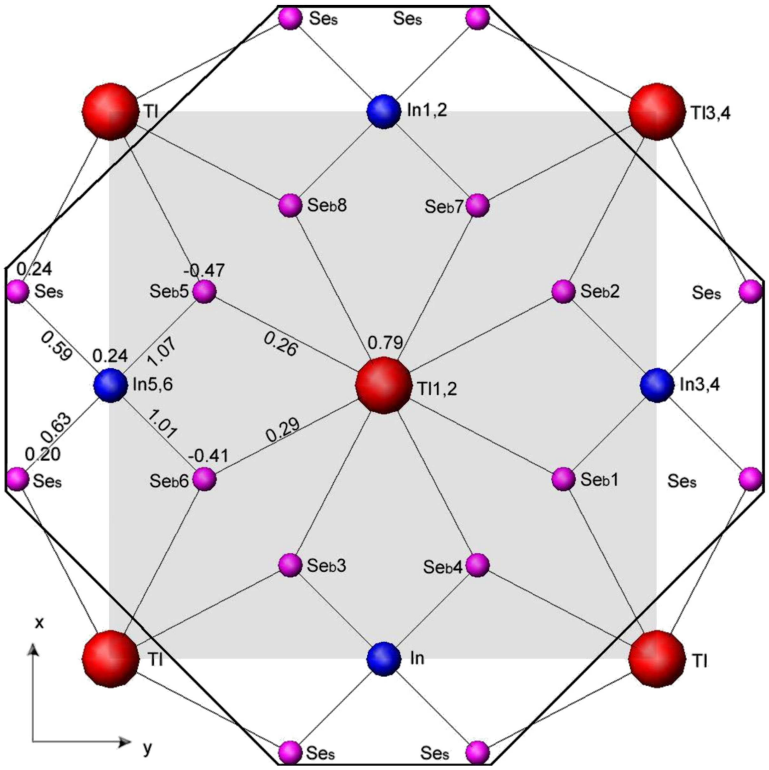

Fig. 1. The $TlIn_4Se_{16}$ cluster as a molecular model (octagon) of $TlInSe_2$ crystal on the xy plane (in shadow). The calculated bond strengths and atom's Löwdin charges are shown in the picture. They are different in different planes from the surface and reveal themselves in the VB and CL electronic structure.

The diagonal matrix ε gives the energies of MO levels. For the core levels they nearly correspond to the energy of the AO levels. However, due to interaction they are slightly diffused. Fock matrix elements $F^{\alpha}_{\mu\nu}$ and overlap integrals $S_{\mu\nu}$ are obtained *ab initio* in the following way:

$$F^{\alpha}_{\mu\nu} = H_{\mu\nu} + \frac{1}{2}\sum_{k,\lambda=1}^{M}\Big\{\big(\langle\mu\nu|k\lambda\rangle - \langle\mu k|\nu\lambda\rangle\big)P^{\alpha}_{k\lambda} + \langle\mu\nu|k\lambda\rangle P^{\beta}_{k\lambda}\Big\}\,, \tag{5}$$

$$S_{\mu\nu} = \int \chi_\mu\,\chi_\nu\,\mathrm{d}\mathbf{r}\,, \tag{6}$$

where

$$H_{\mu\nu} = \int \chi_\mu\left(-\frac{1}{2}\Delta - \sum_A \frac{Z_A}{|\mathbf{r}-\mathbf{r}_A|}\right)\chi_\nu\,\mathrm{d}\mathbf{r} \tag{7}$$

are the matrix elements of the kinetic energy of an electron and its interaction with the nucleus Z_A. The energy of the interaction between two electrons is given by

$$\langle\mu\nu|k\lambda\rangle = \iint \frac{\chi_\mu(\mathbf{r}_1)\chi_\nu(\mathbf{r}_1)\chi_k(\mathbf{r}_2)\chi_\lambda(\mathbf{r}_2)}{|\mathbf{r}_1-\mathbf{r}_2|}\,\mathrm{d}\mathbf{r}_1\,\mathrm{d}\mathbf{r}_2\,. \tag{8}$$

The coefficients $C_{i\mu}$ allow one to calculate the electronic structure of molecules and to interpret the experimental results. They also allow us to find the matrix of the electron distribution density, which is given by

$$P^{\alpha}_{\mu\nu} = \sum_{i=1}^{N_\alpha} C^{\alpha}_{i\mu}C^{\alpha}_{i\nu}\,, \tag{9}$$

$$P^{\beta}_{\mu\nu} = \sum_{i=1}^{N_\beta} C^{\beta}_{i\mu}C^{\beta}_{i\nu}\,. \tag{10}$$

Here N_α and N_β are the numbers of electrons with spins α and β, respectively. Equations (3) and (4) are solved by Fock matrix $\mathbf{F}$ diagonalisation. The orthogonalisation of this matrix was proposed by Löwdin in a following way:

$$\mathbf{C} = \mathbf{S}^{-1/2}\mathbf{C}_0\,. \tag{11}$$

As Fock matrix elements (Eqs. (3), (4)) nonlinearly depend on unknown coefficients $C_{i\mu}$, UFR equations are solved by iteration.

According to Löwdin the density matrix $\mathbf{P}$ has to be renormalized in this way:

$$\mathbf{P} = \mathbf{S}^{1/2}\mathbf{P}\mathbf{S}^{1/2}\,. \tag{12}$$

Having the MO coefficients **C** (Eqs. (1), (2)), one can find bond strengths P_{AB} between the atoms A and B

$$P_{AB} = \sum_{\sigma\in A}\sum_{\lambda\in B}(P^{\alpha}_{\sigma\lambda} + P^{\beta}_{\sigma\lambda})\,, \qquad (13)$$

and the charges of atoms

$$q_A = Z_A - \sum_{\mu\in A}(P^{\alpha}_{\mu\mu} + P^{\beta}_{\mu\mu})\,. \qquad (14)$$

Knowing the MO coefficients $\mathbf{C}_0$ from Eq. (11), one can evaluate the contribution of A atom electrons for ε_i state:

$$p_{iA} = \sum_{\mu\in A}^{M} C^2_{0\,i\mu}\,. \qquad (15)$$

The UHF method was realized with the GAMESS program [11]. In our model (Fig. 1), the calculations have shown that Löwdin charges of atoms are: $Tl^{+0.79}$, $In^{+0.24}$, and $Se^{-0.47}$. The charges of atoms in our model differ from those supposed in [6]. Tl is in an octahedral site, while In is in a tetragonal site and covalently bound with 2 bulk (Se_b) and 2 surface (Se_s) atoms. The charge of surface $Se_s^{+0.24}$ atoms is not compensated by electropositive Tl atoms and it distorts the VB. The calculated bond strengths and atom Löwdin charges are also shown in Fig. 1. The bonds of the surface Se atoms in the cluster are broken and therefore their charges and bond strengths are decreased.

4. Results of the XPS measurements

Figure 2 shows the XPS of the $TlInSe_2$ crystal in the energy range of 0 to 1400 eV below the Fermi level without contamination by any gas and only with a small amount of carbon (C $1s$ peak at 284.5 eV). Auger spectra of Se *LMM*, In *MNN*, and of Tl *NOO* are also seen. Inelastically scattered electrons give the background. XPS did not show any traces of impurities, only the carbon was visible after the sample was cleft under high vacuum conditions, in the low 10^{-10} Torr range. We did not find any noticeable change of the surface composition with time at a fixed temperature as well as the dependence on illumination time. The strongest peaks of Tl $4f$, I $3d$, and Se $3d$ were chosen for investigating peculiarities of the core-level XPS.

4.1. XPS of the valence band

Figure 3 shows the VB spectrum. This spectrum is referred to the Fermi level (E_F). The E_F was defined with the accuracy of 0.3 eV. The VB is separated by a gap of about 0.6 eV (crosswise) and 1.0 eV at room temperature or 0.6 eV at 393 K (lengthwise) from the Fermi level and it extends down to 10 eV below the E_F. Above

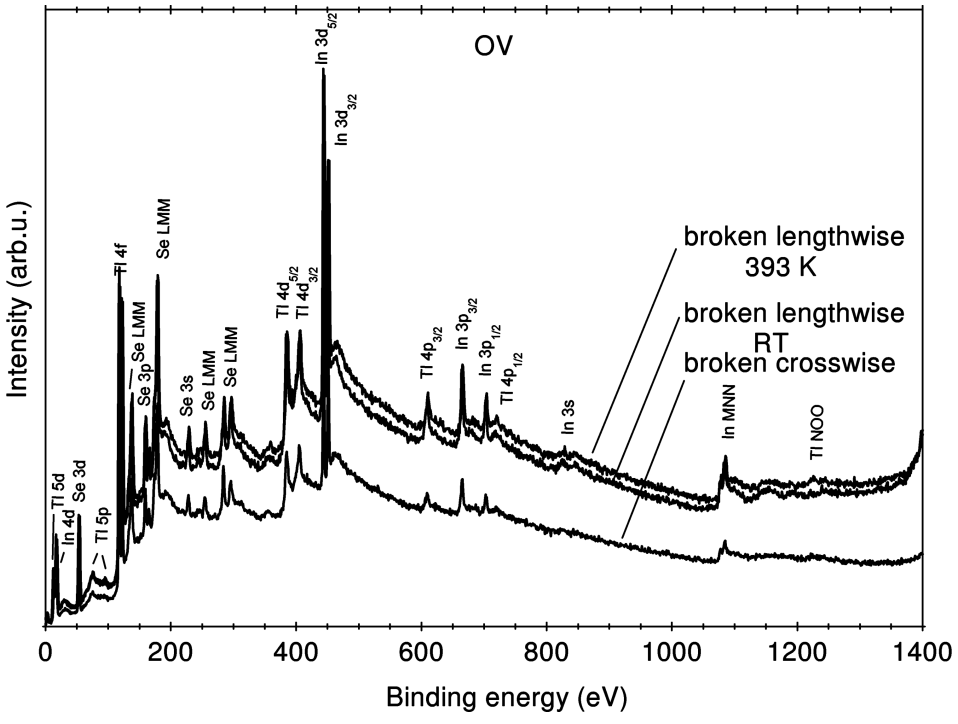

Fig. 2. XPS of $TlInSe_2$ crystal (010) and (001) surfaces in the energy range 0 to 1400 eV.

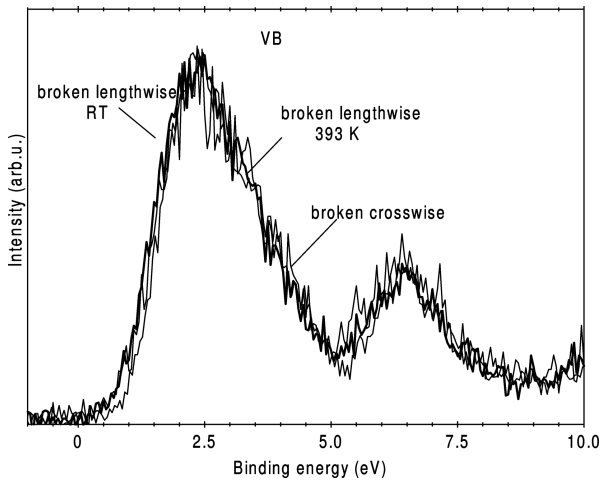

Fig. 3. XPS of the valence band.

Table 2. Binding energies and chemical shifts of atoms of different surfaces.

Peak	Binding energy (eV)		
	broken crosswise	broken lengthwise, RT	broken lengthwise, 393 K
Tl $4f_{7/2}$ in compound	118.5	118.3	118.3
Tl $4f_{7/2}$ in literature		117.7	
chemical shift	0.8	0.8	0.6
In $3d_{5/2}$ in compound	444	444.5	444.3
In $3d_{5/2}$ in literature		443.9	
chemical shift	0.1	0.6	0.4
Se $3d_{5/2}$ in compound	53.4	53.6	53.5
Se $3d_{5/2}$ in literature		55.6	
chemical shift	-2.2	-2.0	-2.1

10 eV, the CL of Tl $5d$ and In $4d$ are the closest to VB. In these crystals, the calculated room temperature direct band gap is about 0.6 eV while optical absorption data favour indirect transitions at band gap of 1.2 eV [12]. These values almost correspond to the values obtained by the XPS measurements.

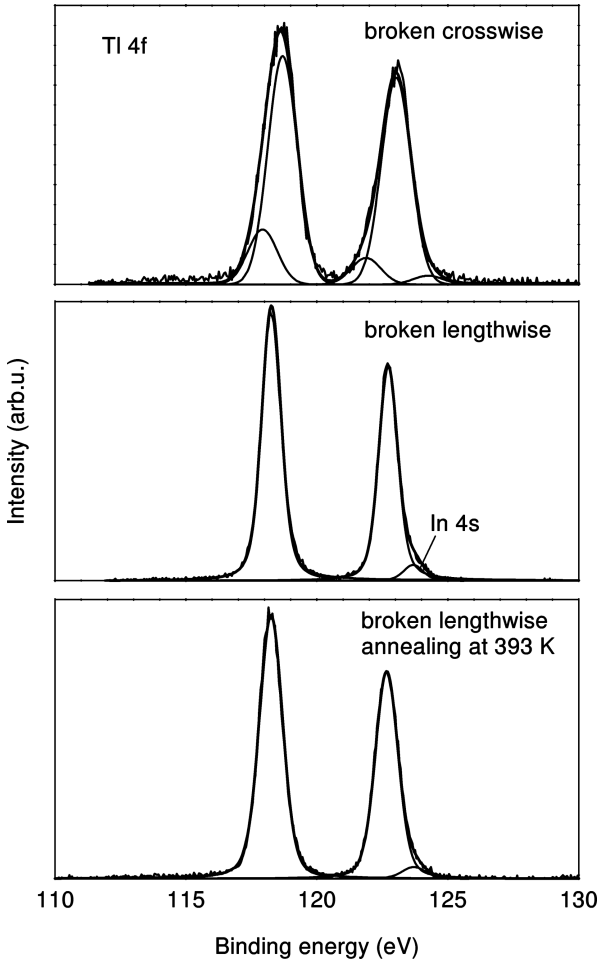

Fig. 4. XPS of Tl $4f_{7/2}$ and $4f_{5/2}$ spin–orbit doublet. The closest lines are the experimental (solid) and the fits (thin) in Figs. 3–6.

4.2. XPS of the core levels

Figure 4 shows the spectrum of the Tl $4f$ spin–orbit doublet (overlapping by the In $4s$) from the broken lengthwise (010) and crosswise (001) planes. The core-level binding energy, $E_{\rm b}$, is referred (in all figures) to the Fermi level. The peaks of Tl $4f_{7/2}$ are situated at about 118.5 (crosswise) and 118.3 eV (lengthwise), respectively. The chemical shift is 0.8 eV.

Figure 5 shows the spectrum of the spin–orbit doublet of In $3d$. The peaks of In $3d_{5/2}$ are situated at 444.0 and 444.5 eV for crosswise and lengthwise planes, respectively. The chemical shift is 0.1 eV (crosswise) and 0.6 eV (lengthwise). Table 2 shows the binding energies of Tl, In, and Se states in $TlInSe_2$ crystal and pure elements as well as the chemical shifts.

The spectrum of the spin–orbit doublet of Se $3d$ is shown in Fig. 6. The peaks of Se $3d_{5/2}$ are situated at 53.4 and 53.6 eV for crosswise and lengthwise planes, respectively. The chemical shift is -2.2 eV (crosswise) and 2.0 eV (lengthwise).

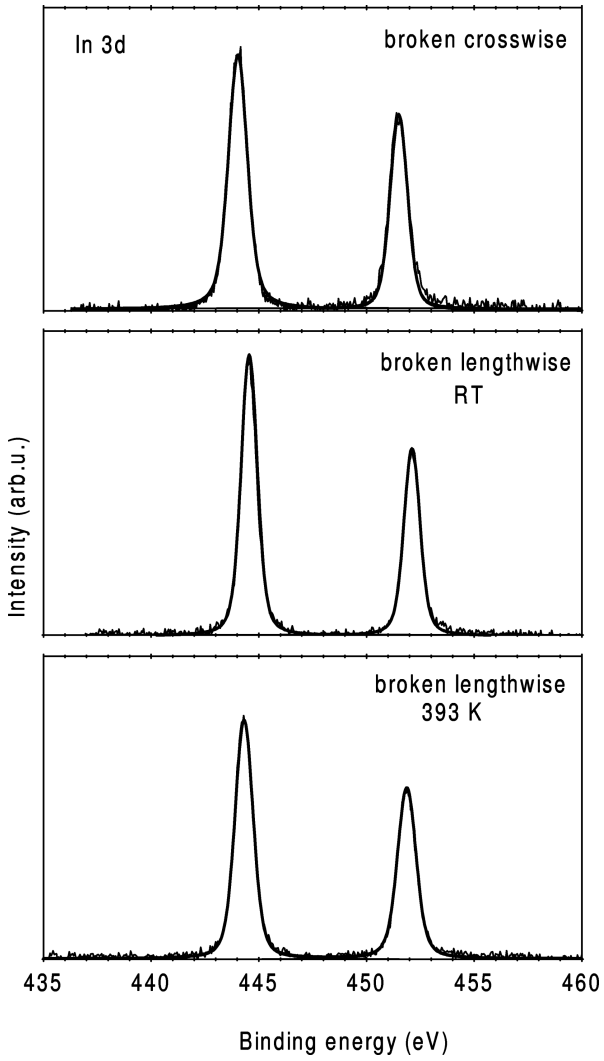

Fig. 5. XPS of In $3d_{5/2}$ and $3d_{3/2}$ spin–orbit doublet.

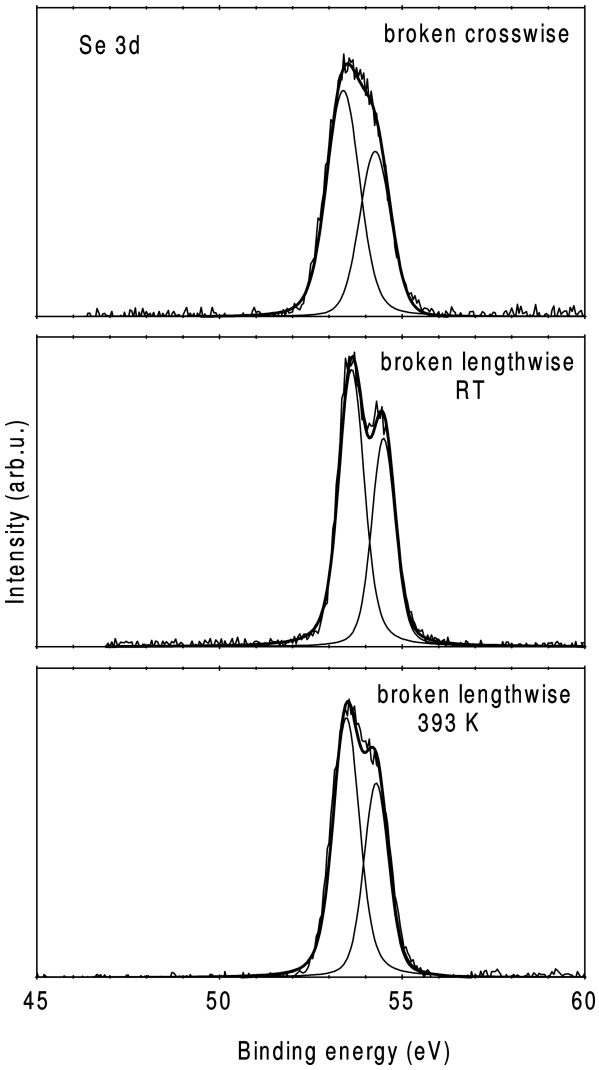

Fig. 6. XPS of Se $3d_{5/2}$ and $3d_{3/2}$ spin–orbit doublet.

Thus, the electronic structure measurements revealed the chemical shift of Tl states of $+0.8$ eV and In states of $+(0.1$–$0.6)$ eV to a higher binding energy, and Se states of $-(2.2$–$2.0)$ eV to a lower binding energy. This shift suggests a charge transfer from Tl and In to Se. The chemical shifts in ferroelectric $TlInS_2$ are comparable [8]. As a result, the both crystals possess similar ionicity, however, the $TlInSe_2$ has no phase transitions and is not a ferroelectric one.

The crosswise spectra of In and Se spin–orbit doublets are wider than the lengthwise spectra. This indicates the stronger interactions and higher bond strengths along the [001] axis (chain axis). But Tl $4f$ spin–orbit doublet is split into two components as in an incommensurate phase of ferroelectric $TlInS_2$ [8]. All the lengthwise spectra from the (010) plane are similar at room temperature and 393 K. They show that there is no phase transition (contrary to supposed earlier in literature) which would change the interactions in this temperature range.

After breaking the crystal under high-vacuum conditions, strong bonds of the surface atoms become open. Due to the reduced coordination number, the surface atoms experience a different potential than the bulk atoms. As a result, the bond strength at surface increases at the expense of broken bonds. Löwdin charges mainly change only for electronegative atoms. The charges of surface atoms compensate the electron density of the broken bonds along the [001] axis. Experimentally it looks as if the surface experiences a different concentration of atoms and different chemical composition (Table 3).

Table 4 presents the theoretical values of the binding energies, calculated with MIDI basis set without taking into account the spin–orbit interaction, and experimentally obtained energies, $E_{\mathrm{b\,exp}}$. The quantum me-

Table 3. Chemical composition and atomic concentration at different surfaces.

Element	Chemical composition		
	broken cross-wise	broken lengthwise, RT	broken lengthwise, 393 K
Tl	0.98	1.04	1.05
In	1.03	1.08	1.07
Se	1.99	1.88	1.88
Peak	**Atomic concentration**		
	broken cross-wise	broken lengthwise, RT	broken lengthwise, 393 K
Tl $4f$	24.5	26.0	26.2
In $3d_{5/2}$	25.7	26.9	26.7
Se $3d$	49.8	47.1	47.1

Table 4. Mean theoretical values of CL, VB (negative), and CB (positive) binding energies for $TlIn_4Se_{16}$ molecular cluster and experimental values for $TlInSe_2$ crystal.

Band	State	$-E_{\mathrm{b\,min}}$, $-E_{\mathrm{b\,max}}$ [eV]	E_{b} (experimental) [eV]
CL	In $3s$	800.3, 800.3	830
	Tl $4s$	724.4, 724.5	
	In $3p$	684.5, 684.6	670–710
	Tl $4p$	617.0, 617.1	620–730
	In $3d$	470.7, 470.8	444–450
	Tl $4d$	419.6, 419.7	390–410
	Se $3s$	233.6, 237.3	230
	Se $3p$	171.7, 175.8	160–170
	Tl $4f$	145.6, 145.7	118–124
	In $4s$	131.7, 131.8	
	Tl $5s$	121.7, 121.8	
	In $4p$	91.8, 91.9	
	Tl $5p$	84.3, 84.4	75–100
	Se $3d$	60.6, 64.5	53–55
	In $4d$	25.3, 25.6	16.7–17.5
	Tl $5d$	22.8, 23.0	12.1–14.4
VB (s)	Se $4s$	21.5, 24.6	5.2–10.0
VB (sp)	In $5s$	6.2, 14.3	0.6–5.2
	$\mathrm{Se_s}$ $4p$		
	Tl $6p$		
	$\mathrm{Se_b}$ $4p$		
CB (p)	$\mathrm{Se_b}$ $4p$	2.8, 5.2	
	In $5p$		
	Tl $6p$		

chanical method and the chosen model give higher negative CL energies than their experimental values. Nevertheless, the model reflects the electronic structure and binding energies of the crystal.

5. Discussion

Theoretical UHF calculations express the ionisation potential with its zero at the vacuum level, while the experimental binding energies refer to the Fermi level. As the energy gap of $TlInSe_2$ is about 0.6 eV, in order to compare the experimental and theoretical binding energies and to refer to the Fermi level we have decreased the calculated ionisation potential by the work function $\phi = 5.2$ eV. Also, UHF method neglects the spin–orbit interactions. Nevertheless, theoretical eigenvalues of CL differ from experimental ones by about 10% and qualitatively explain the XPS (Table 4). Some discrepancy appears because (*i*) a limited basis set of AO for obtaining a molecular orbital solution is used (the cluster $TlIn_4Se_{16}$ as the crystal model), (*ii*) screening and relaxation effects are not taken into account. The relaxation processes are reflected by Auger spectra (Fig. 2). Nevertheless, Koopmans' theorem provides an invaluable tool in assigning XPS.

The VB is located at 0.6 to about 10 eV below the Fermi level. The electronic structure of VB is calculated from Eqs. (3) and (4). It consists of two bands – the intensive sp and less intensive s one. Figure 7 shows the comparison of calculated VB structure of $TlInSe_2$ crystal model with the experimental XPS spectrum up to 10 eV. At higher energies the VB overlaps with the Tl $5d$ and In $4d$ core level energies which Kilday et al. [6] have included into VB. The intensities of the XPS were described in three ways:

- by the energy states band ε_i from the characteristic Eqs. (2) and (3);
- by the peaks of the density of states (DOS):

$$D(\varepsilon) = \frac{1}{N_M}\frac{1}{\Delta\varepsilon}\,, \tag{16}$$

  where N_M is the number of molecules in the cluster;
- by the Gaussian broadening method [12]:

$$D(\varepsilon) = \frac{1}{\sqrt{2\pi\sigma}}\sum_i \exp\left(-\frac{(\varepsilon-\varepsilon_i)^2}{2\sigma^2}\right), \tag{17}$$

  where the sum is performed over the states i, ε_i are the corresponding energy levels, and σ is the energy broadening parameter.

Every way has some advantages and shortcomings. The first way is self-evident but it does not provide qualitative band form evaluation. The second one gives quantitative evaluation density of states, however, it overestimates the intensity of degenerate or close states. The Gaussian broadening method describes the integral

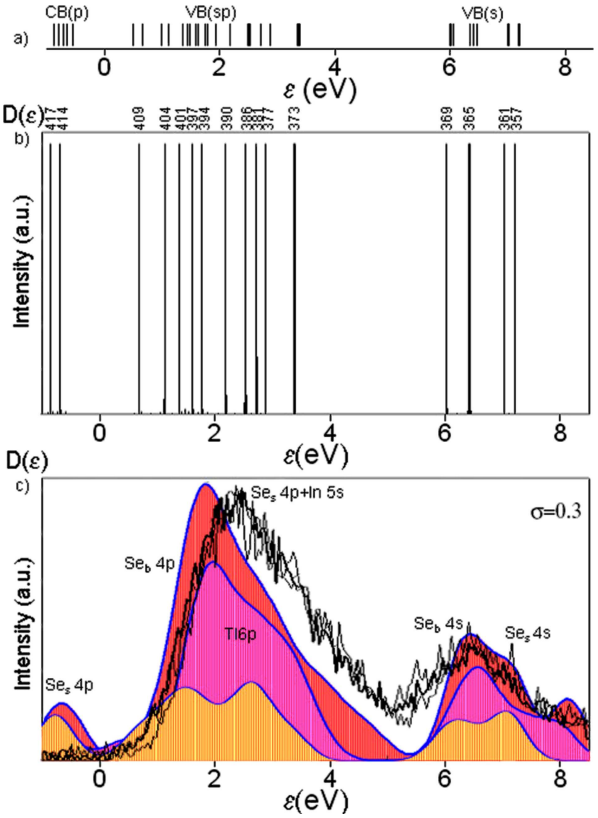

Fig. 7. Electronic structure of VB. DOS band of the $TlIn_4Se_{16}$ cluster (upper panel), intensity of DOS and MOs are indicated in the middle panel (numbers correspond to MOs shown in Table 5). VB spectra approximation by the Gaussian broadening method of three different clusters, $TlIn_4Se_{16}$ (lower part), $Tl_3In_6Se_{24}$ (middle part), and $Tl_7In_{10}Se_{40}$ (upper curve) and their comparison with experimental XPS are shown in the bottom.

form of the band which is close to the experimental one, however, it does not show the structure of DOS.

Further, all experiments have a finite-energy resolution and frequently concentrate on the shifts, distortions, and changes in weight in the spectral features. In the approach used (Eq. (17)), the aim was to calculate the DOS only at the high density of k-points and then to smear the resulting spectrum to the experimental resolution. However, the application of the Gaussian smearing to the DOS results in a good convergence at low k-point sampling densities.

Figure 7 presents the form and electronic structure of $TlInSe_2$ crystal model which are similar to those calculated by a pseudo-potential method [13]. The top of the figure represents $D(\varepsilon)$ (Eq. 16) for the peaks of the DOS. In the middle panel of the figure the intensities of DOS and MOs of Tl, In, and Se atoms are shown. Experimental XPS is the integral picture of all electronic states. At the bottom of the figure the approximation of $TlInSe_2$ bands spectra of three different clusters by the Gaussian broadening method (Eq. (17)) and their comparison with experimental XPS are presented. The theoretical VB is compressed.

Table 5. Population (in %) of VB levels in $TlIn_4Se_{16}$ cluster. Se_b and Se_s are bulk and surface atoms. VB binding energies are negative, while CB ones are positive. VB binding energies are shifted towards E_F by work function.

ε_i [eV]		MO_i	Tl	In	Se_b	Se_s
CB (p)	0.9	417	4	6	19	71
	0.7	414	0	4	5	91
VB (sp)	0.5	411	1	7	71	21
	0.7	409	0	6	73	21
	1.1	404	0	4	90	6
	1.4	401	1	6	83	10
	1.6	397	2	16	74	8
	1.8	394	7	7	72	14
	2.2	391	0	25	58	17
	2.5	386	0	14	3	83
	2.5	385	27	5	65	3
	2.7	381	0	3	2	95
	2.9	377	0	6	4	90
	3.4	373	0	34	14	52
VB (s)	6.0	369	0	8	91	1
	6.4	365	0	7	89	4
	7.0	361	0	4	0	96
	7.7	357	1	5	5	89

The VB electronic structure is seen also from Table 5 in which an analysis of the contribution of atom electrons for ε_i state is calculated by Eq. (15). Se bulk (73%) and surface (21%) atoms' degenerate $4p$ states (MO 409) form a sharp left side (near to E_F) of the sp band. In $5s$ and surface Se $4p$ states form a right side (MOs 377, 381) of sp band. Tl $6p$ states form the middle part of sp band, while bulk (MO 365) and surface (MOs 361, 357) Se $4s$ states form the s band. Surface Se $4p$ states (MOs 414–417) form the CB p band.

Theoretically all the CL are split due to electron–electron interaction with the electrons of other layers. Experimentally only Tl $4f$ (broken crosswise) doublet is split as if the surface and bulk atoms were in different valence states.

6. Conclusions

For the first time the form and electronic structure of the valence band of the $TlInSe_2$ crystal was studied experimentally and calculated by solving the UHF matrix equations. Only quasi-two-dimensional molecular cluster perpendicular to the c axis is stable according to UHF equations. UHF method gives about 10% higher CL binding energies and twice wider VB than the ex-

perimental values seemingly due to overestimation of the exchange electron interaction.

The VB is composed of the s and sp bands. Bulk and surface Se $4s$ states form the s band. Se $4p$, In $5s$ and $5p$, Tl $6s$ and $6p$ states form the sp band: Se $4p$ states form the sharp left side while In $5s$ and surface Se $4p$ states form the right side. Se $4p$ surface states form the conduction band.

No structural changes have been found in the studied temperature range.

References

[1] J. Grigas, *Microwave Dielectric Spectroscopy of Ferroelectrics and Related Materials* (OPA Gordon and Breach, Amsterdam, 1996).

[2] G. Margaritondo, in: *Physics and Chemistry of Materials with Low Dimensional Structure – Electronic Structure and Electronic Transitions in Layer Materials: Recent Developments*, Vol. 20, ed. V. Grasso (Reidel, Dordrecht, 1986) p. 6.

[3] M. Hanias, A.N. Anagnostopoulos, K. Kambas, and J. Spyridelis, I–U dependence of $TlInX_2$ (X = Se, Te) crystals: The ohmic and S-type regions, Phys. Rev. B **43**, 4135–4140 (1991).

[4] C. Karakotsou and A.N. Anagnostopoulos, Crisis in electrical behaviour of the $TlInSe_2$ semiconducting compound, Physica D **93**, 157–164 (1996).

[5] L. Porte and A. Tranquard, Spectroscopie photoelectronique (XPS) de calcogenures de thallium, J. Solid State Chem. **35**, 59–68 (1980).

[6] D.G. Kilday, D.W. Niles, G. Margaritondo, and F. Lewy, Electronic structure of the chain chalcogenide $TlInSe_2$, Phys. Rev. B **35**, 660–663 (1987).

[7] J. Grigas, E. Talik, and V. Lazauskas, X-ray photoelectron spectra and electronic structure of Bi_2S_3 crystals, Phys. Status Solidi B **232**, 220–230 (2002).

[8] J. Grigas and E. Talik, Splitting of X-ray photoelectron spectra in incommensurate ferroelectric $TlInS_2$ crystals, Phys. Status Solidi B **237**, 494–499 (2003).

[9] V. Lazauskas, V. Nelkinas, J. Grigas, E. Talik, and V. Gavryushin, Electronics structure of valence band of ferroelectric SbSI crystals, Lithuanian J. Phys. **46**, 205–210 (2006).

[10] D. Müller, G. Eulenberger, and H. Hahn, Über ternäre Thalliumchalkogenide mit Thalliumselenidstruktur, Z. Anorg. Allg. Chem. **398**, 207–220 (1973).

[11] M.W. Schmidt, K.K. Baldrige, J.A. Boatz, S.T. Elbert, M.S. Gordon, J.H. Jensen, S. Koseki, N. Matsunaga, K.A. Nguyen, S. Su, T.L. Windus, M. Dupuis, and J.A. Montgomery, General atomic and molecular electronic structure system, J. Comput. Chem. **14**, 1347–1363 (1993).

[12] C.J. Pickard and M.C. Payne, Extrapolative approaches to Brillouin-zone integration, Phys. Rev. B **59**, 4685–4693 (1999).

[13] G. Orudzev, N. Mamedov, H. Uchiki, N. Yamamoto, A. Iida, H. Toyota, E. Gojaev, and F. Hashimzade, Band structure and optical functiona of ternary chain $TlInSe_2$, J. Phys. Chem. Solids **64**, 1703–1706 (2003).

$TlInSe_2$ KRISTALŲ RENTGENO FOTOELEKTRONŲ SPEKTRAI IR ELEKTRONINĖ SANDARA

J. Grigas [a], E. Talik [b], M. Adamiec [b], V. Lazauskas [c], V. Nelkinas [c]

[a] *Vilniaus universitetas, Vilnius, Lietuva*
[b] *Silezijos universitetas, Katovicai, Lenkija*
[c] *Vilniaus universiteto Teorinės fizikos ir astronomijos institutas, Vilnius, Lietuva*

Santrauka

Pateikti $TlInSe_2$ monokristalų Rentgeno (Röntgen) spindulių sužadintų fotoelektronų iš (010) bei (001) plokštumų valentinės juostos (VJ) ir svarbiausių gilių lygmenų spektrai. Fotoelektronų sužadinimo šaltinis buvo Al K_α 1486,6 eV monochromatinė spinduliuotė. Sužadintų fotoelektronų spektrai matuoti energijos srityje nuo 0 iki 1400 eV. Eksperimentiškai gautos fotoelektronų energijos palygintos su teorinių *ab initio* skaičiavimų rezultatais. Apskaičiuota ir eksperimentiškai patvirtinta kristalo VJ sandara. VJ yra nuo 0,6 iki 10 eV ir sudaryta iš sp ir s juostų, kurios savo ruožtu sudarytos iš atitinkamai Se $4p$ + In $5s$, Tl $6p$ ir Se $4s$ juostų. Parodyta, kokie paviršiaus ir tūrio atomai lemia VJ formą. Įvertinti atomų elektros krūviai ir ryšio stipriai. Apskaičiuotasis būsenų tankis ir VJ forma artimi eksperimentiškai išmatuotiems. Nustatyti Tl, In ir Se atomų cheminiai poslinkiai.